Biomech Model Mechanobiol (2017) 16:1925–1936
DOI 10.1007/s10237-017-0928-0

ORIGINAL PAPER

Estimation of the effective yield properties of human trabecular bone using nonlinear micro-finite element analyses

Patrik Wili[1] · Ghislain Maquer[1] · Jarunan Panyasantisuk[1] · Philippe K. Zysset[1]

Received: 22 February 2017 / Accepted: 9 June 2017 / Published online: 22 June 2017

Abstract Micro-finite element (μFE) analyses are often used to determine the apparent mechanical properties of trabecular bone volumes. Yet, these apparent properties depend strongly on the applied boundary conditions (BCs) for the limited size of volumes that can be obtained from human bones. To attenuate the influence of the BCs, we computed the yield properties of samples loaded via a surrounding layer of trabecular bone ("embedded configuration"). Thirteen cubic volumes (10.6 mm side length) were collected from μCT reconstructions of human vertebrae and femora and converted into μFE models. An isotropic elasto-plastic material model was chosen for bone tissue, and nonlinear μFE analyses of six uniaxial, shear, and multi-axial load cases were simulated to determine the yield properties of a subregion (5.3 mm side length) of each volume. Three BCs were tested. Kinematic uniform BCs (KUBCs: each boundary node is constrained with uniform displacements) and periodicity-compatible mixed uniform BCs (PMUBCs: each boundary node is constrained with a uniform combination of displacements and tractions mimicking the periodic BCs for an orthotropic material) were directly applied to the subregions, while the embedded configuration was achieved by applying PMUBCs on the larger volumes instead. Yield stresses and strains, and element damage at yield were finally compared across BCs. Our findings indicate that yield strains do not depend on the BCs. However, KUBCs significantly overestimate yield stresses obtained in the embedded configuration (+43.1 ± 27.9%). PMUBCs underestimate (−10.0 ± 11.2%), but not significantly, yield stresses in the embedded situation. Similarly, KUBCs lead to higher damage levels than PMUBCs (+51.0 ± 16.9%) and embedded configurations (+48.4 ± 15.0%). PMUBCs are better suited for reproducing the loading conditions in subregions of the trabecular bone and deliver a fair estimation of their effective (asymptotic) yield properties.

Keywords Nonlinear micro-FEA · Trabecular bone · Yield properties · Damage · Embedded configuration

✉ Ghislain Maquer
ghislain.maquer@istb.unibe.ch

[1] Institute for Surgical Technology and Biomechanics, University of Bern, Bern, Switzerland

1 Introduction

Osteoporosis is a bone condition accountable for a higher fracture risk among the elderly (Ray et al. 1997). Better understanding of the etiology of osteoporotic fractures and new criteria for fracture risk evaluation are necessary to prevent them more efficiently. Bone strength has the potential to become a more reliable contributor to fracture risk (Qasim et al. 2016) and can be assessed by numerical techniques such as continuum-based homogenized finite element (hFE) models. In fact, computed tomography (CT)-based hFE modeling slowly makes its way toward clinical applications. An example is monitoring of treatment-related changes of bone strength (Zysset et al. 2015).

Following homogenization theory (Hollister et al. 1991), hFE simulations are based on relationships between the averaged mechanical and structural characteristics of trabecular volumes (Cowin 1985; Zysset 2003). Both aspects can be obtained from μCT images either via metrics characterizing the trabecular network, mainly bone volume fraction and fabric anisotropy, or by performing μFE analyses providing elastic and yield properties (Rietbergen et al. 1995; Maquer et al. 2015; Musy et al. 2017). Such numerical analysis allows the same sample to be tested under different loading scenarios without being damaged as in experiments.

Homogenization relies on the concept of a representative volume element (RVE), the smallest subvolume that can be considered large enough to be statistically representative of the material's microstructure (Hill 1963). If such an RVE can be defined for a medium, it can be used to calculate its effective (or asymptotic) mechanical properties that are independent of the applied boundary conditions (BCs). In turn, this RVE must be small with respect to the dimensions of the structure to be analyzed by homogenized FE. For a periodic medium, the primary choice for the RVE is the smallest periodic unit cell, which effective mechanical properties can be calculated using periodic BCs. For a partially random medium such as trabecular bone, periodic BCs do not make sense and the apparent mechanical properties computed with other BCs may not be effective if the size of the analyzed volume element (VE) is too small (Hazanov and Huet 1994). For many years, a trabecular VE with a characteristic length of five trabecular lengths (∼4 mm) was thought to be large enough (Harrigan et al. 1988). Yet, the apparent mechanical properties obtained for typical trabecular VEs of 4–5 mm depend on the applied boundary conditions and these VEs are therefore not representative (Pahr and Zysset 2008). These boundary effects decrease with the size of the VE, but the size of trabecular regions with a homogenous microstructure is *anatomically* limited. Three classes of BCs fulfill Hill's condition (equivalence of micro- and macro-level strain energies) for non-periodic media (Hill 1963). Kinematic uniform BCs (KUBCs) impose uniform displacements to the nodes of the boundary, static uniform BCs (SUBCs) that impose uniform tractions, and mixed uniform BCs (MUBCs), a combination of uniform displacements and tractions. Pahr and Zysset (2008) thus introduced periodicity-compatible MUBCs (PMUBCs), a special set of MUBCs that can be applied on nearly orthotropic microstructures (e.g., trabecular bone) to mimic the periodic BCs successfully used to compute the effective mechanical properties of periodic media. Daszkiewicz et al. (2017) recently introduced another option: the "embedded configuration." Instead of loading the trabecular volume directly, the volume remains "in situ," and the load is transmitted via the surrounding layer of trabecular bone to minimize the influence of the BCs. The obtained properties indeed approximated the effective elastic properties of the samples, when the surrounding layer was thicker than 2 mm and were close to the apparent properties computed with PMUBCs. However, this work relied on linear μFE simulations, which limited the findings to the elastic properties.

We therefore propose to translate the idea of embedded configuration to nonlinear μFE models to estimate the effective yield properties of thirteen trabecular bone samples obtained from human femora and vertebrae (Fig. 1a). Our first hypothesis is that the yield properties obtained from embedded samples are independent of the outer BCs if the surrounding layer is thicker than 2 mm (Fig. 1b). Our second hypothesis is that PMUBCs are able to mimic the yield stresses obtained from the embedded configuration better than KUBCs (Fig. 1c). Our last hypothesis is that PMUBCs induce similar damage distribution as the embedded configuration, unlike KUBCs (Fig. 1d).

2 Materials and methods

2.1 Sample preparation

Micro-computed tomography images (36 μm voxel size) of human vertebral bodies (4 male and 2 female donors, 70 ± 6.5 years) and femoral heads (2 female donors, 81 and 95 years) were obtained from two previous studies (Lochmüller et al. 2008; Marangalou et al. 2013). The ethical approval for collection and preparation of the vertebrae was obtained by the Institute of Anatomy of the LMU Munich, while the Institute of Anatomy of the Amsterdam Medical Center took care of the femoral heads.

More details about the pre-processing of the data can be found in Daszkiewicz et al. (2017). Briefly, 13 large cubic volume elements (CVEs) (10.6 mm side length) were extracted from the μCT reconstructions (six from the vertebra data, seven from the femur data). The marrow phase was not included in the models. The bone phase of the CVEs was segmented via a single-level threshold and their fabric tensor was evaluated with the mean intercept length (Harrigan and Mann 1984). The CVEs were then tilted to align their orthogonal edges with the eigenvectors of the fabric tensor. Those large CVEs were only used for the embedded configuration of small CVEs (5.3 mm side length) located in their core (Fig. 1a). Those 5.3 mm cubes were then cropped from the large ones for the direct computation of apparent yield properties with KUBCs and PMUBCs. Prior works motivated the sample size and the voxel size. For instance, Pahr and Zysset (2008) recommend using CVEs larger than 5 mm edge length to be both nearly orthotropic and representative of the trabecular microstructure. Using 10.6 mm CVEs to evaluate 5.3 mm subCVEs under embedded conditions was decided upon by Daszkiewicz et al. (2017) who showed that the elastic properties could be considered effective if the outer trabecular layer was thicker than 2 mm (2.6 mm in our case).

In terms of morphology (Table 1), bone volume fraction (BV/TV) of the small and large CVEs and that of the surrounding layers were evaluated. The degree of anisotropy (DA) of the small and large CVEs was defined as the ratio between the largest and smallest eigenvalue of the fabric tensor.

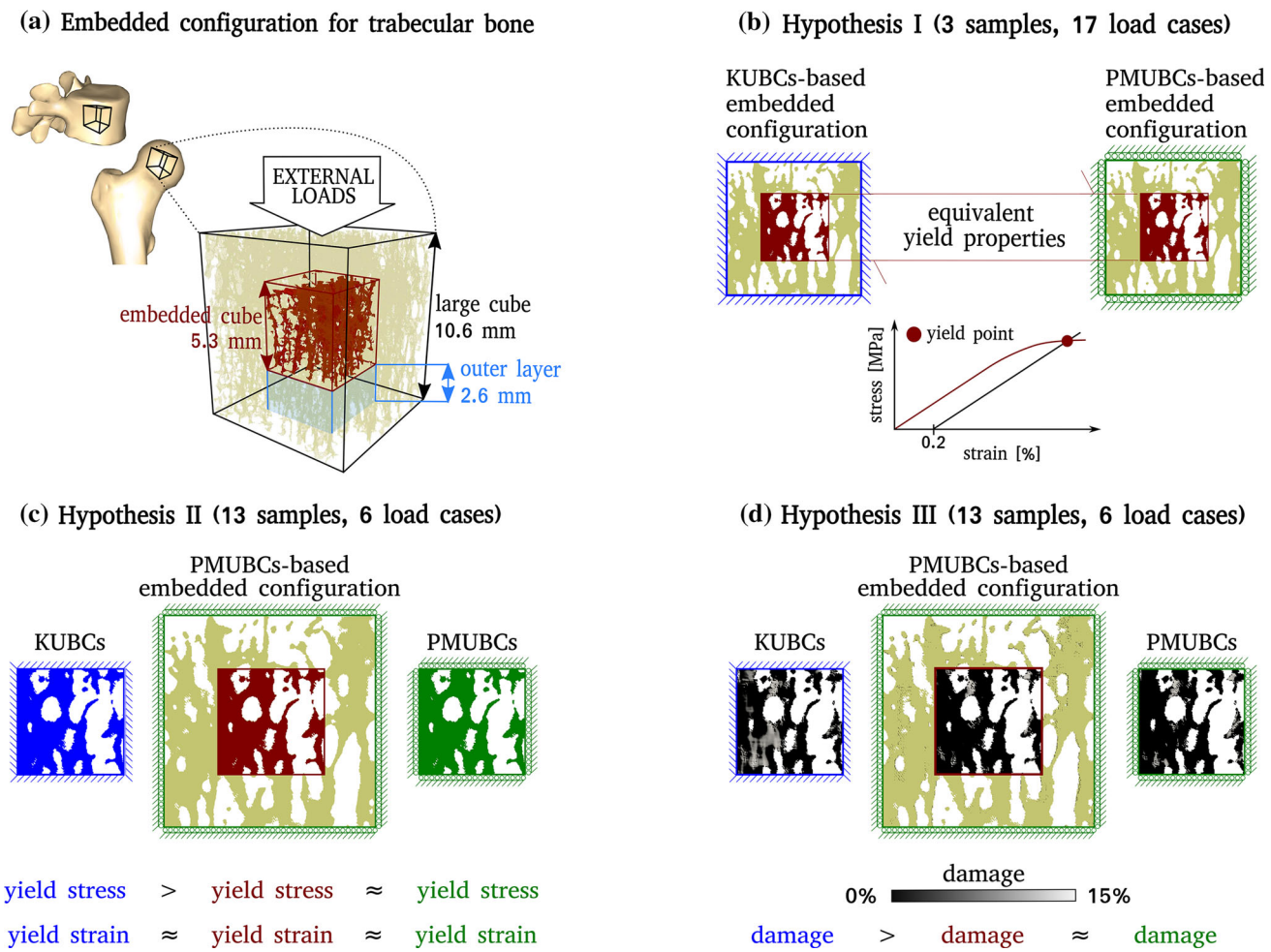

Fig. 1 **a** Thirteen large cubic samples (10.6 mm) were extracted from micro-CT reconstructions (36-μm voxel size) of human femoral heads and vertebral bodies in the trabecular region. The embedded configuration proposed by Daszkiewicz et al. (2017) for trabecular bone was used to evaluate the yield behavior of cubes (5.3 mm) loaded via an outer layer of bone (2.65 mm thickness) and address three hypotheses. **b** Hypothesis I: The yield behavior of the embedded cubes is not affected by the BCs applied on the outer layer if this one is thicker than 2 mm. **c** Hypothesis II: Unlike KUBCs, PMUBCs applied directly on the 5.3 mm cubes lead to similar yield stresses than the embedded configuration, but the yield strains do not depend on the BCs. **d** Hypothesis III: Similar to yield stress, PMUBCs lead to similar damage in the 5.3 mm cube as the embedded configuration, while KUBCs overestimate it

2.2 Computation of the yield strains and stresses using nonlinear micro-FE analyses

μFE models were generated by converting bone voxels into isotropic eight-node hexahedral full integration finite elements. An isotropic elasto-plastic material model was then used to model the mechanical behavior of bone tissue (Schwiedrzik et al. 2016). An elastic modulus of 10 GPa and a Poisson ratio of 0.3 were assigned to each bone tissue element while an approximated Drucker-Prager criterion with tissue yield strain of $\sigma_0^+ = 0.54$ % in tension and $\sigma_0^- = 0.81$ % in compression defined the yield properties (Bayraktar et al. 2004; Schwiedrzik et al. 2016). The material model and its parameters were previously used in nonlinear μFE analyses to simulate compressive and tensile tests of trabecular biopsies up to the post-yield regime (Schwiedrzik et al. 2016).

To assess the yield behavior of trabecular bone volumes, displacement-controlled nonlinear μFE simulations were performed for load cases defined in the subsequent sections. Panyasantisuk et al. (2016) explained the methodology in detail. Each load case was defined by a macroscopic stress characterized by a magnitude (its norm) and one (or several) unit stress direction (∼loading direction). These unit stress directions are given in Table 2. The displacement induced by a given load case was then calculated according to Hooke's law along the unit stress directions that defines the loading directions. The corresponding small-strain tensor could be defined for each sample based on the compliance tensor under KUBCs and PMUBCs (obtained from Daszkiewicz

Table 1 BV/TV and DA of the small and large CVEs and of the corresponding outer layers reflect the morphology of our samples

Anatomical site	BV/TV 5.3 mm CVE (%)	BVTV 10.6 mm CVE (%)	BV/TV outer layer (%)	DA of 5.3 mm CVE (−)	DA of 10.6 mm CVE (−)
vertebra[1]	6.5	6.3	6.0	1.6	1.6
vertebra	7.9	8.8	8.8	1.7	1.5
vertebra	8.1	7.1	6.9	1.7	1.6
vertebra	9.9	9.6	9.5	1.8	1.6
femur	11.6	13.1	13.2	1.4	1.4
vertebra[2]	14.1	12.8	12.5	1.6	1.5
femur	19.7	21.1	21.3	1.5	1.6
femur	21.2	21.6	21.4	1.5	1.4
vertebra	21.3	22.0	22.0	1.1	1.2
femur	22.0	23.7	23.3	1.2	1.3
femur	27.0	24.0	23.6	1.5	1.6
femur[3]	32.2	27.7	27.1	1.7	1.6
femur	39.4	31.1	29.8	1.6	1.7

Yield surfaces were established via 17 load cases for samples 1, 2, and 3

Table 2 Seventeen load cases were used for fitting the yield surfaces of samples 1, 2, and 3 (Table 1)

Load case	Abbreviation	Unit stress direction					
		e1 ⊗ e1	e2 ⊗ e2	e3 ⊗ e3	e1 ⊗ e2	e1 ⊗ e3	e2 ⊗ e3
tensile 1	tens1	S11+					
tensile 2	tens2		S22+				
tensile 3*	tens3			S33+			
compression 1	comp1	S11−					
compression 2	comp2		S22−				
compression 3*	comp3			S33−			
shear 12*	shr12				S12−		
shear 13	shr13					S13	
shear 23*	shr23						S23−
triaxial tens.*	ttens	S11+	S22+	S33+			
multi tens. 1	mten1	S11−	S22+	S33+			
multi tens. 2	mten2	S11+	S22−	S33+			
multi tens. 3	mten3	S11+	S22+	S33−			
multi comp. 1	mcom1	S11+	S22−	S33−			
multi comp. 2	mcom2	S11−	S22+	S33−			
multi comp. 3	mcom3	S11−	S22−	S33+			
triaxial comp.*	tcomp	S11−	S22−	S33−			

Only six (*) were applied to all the other samples. $\pm S_{ij}$ refers to the stress in $e_i = \otimes e_j$ direction where $i, j = 1, 2, 3$

et al. 2017). The displacements to apply to the surfaces of the large and small CVEs were computed by multiplying the small-strain tensor and the dimensions of the CVE.

In our study, the apparent Cauchy stresses of each small CVE loaded under KUBCs and PMUBCs were calculated using volume averages of the infinitesimal Cauchy stress (Pahr and Zysset 2008), which were then projected to the assigned loading direction (Table 2) (Panyasantisuk et al. 2016). Apparent strains were calculated from the known deformations at the boundaries of the CVE according to the applied loads and BCcs. However, for the embedded CVE, there is no a priori knowledge of the local deformations occurring at the faces. In that case, the large CVE was seen as a uniform 3D grid. Each grid point is either a bone node, whose displacements have been calculated, or a "virtual" marrow node, whose displacements have been linearly interpolated from the nearest bone nodes. The displacements of the grid points were averaged for each face of the small inter-

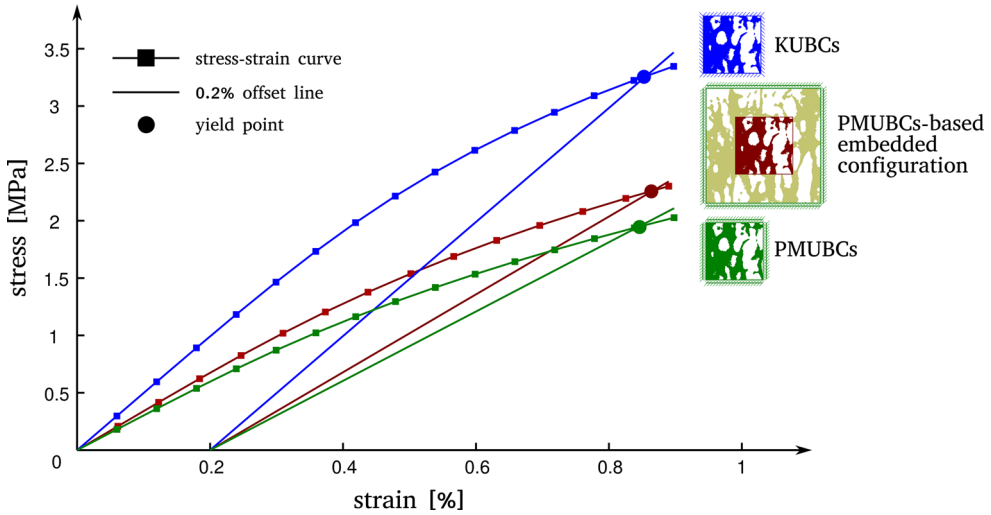

Fig. 2 The yield point was defined as a 0.2 % shift of the apparent elastic strain norm. The *markers* indicate the increments used for the nonlinear analyses. One aim of the study is to compare the yield stresses and yield strains for a cube loaded under three boundary conditions (KUBCs, PMUBCs and PMUBC-based embedded)

nal CVE. An example is given in Daszkiewicz et al. 2017. Yield stresses and strains were finally defined as a 0.2% shift of the projected apparent Cauchy stress and the apparent elastic strain norm (Fig. 2).

The Medtool program (version 4.0, Dr. Pahr Ingenieurs e.U, Austria) generated meshes and BCs. All simulations were performed with the parallel extension of the finite element code FEAP (parFEAP 8.3) (Taylor and Govindjee 2013) on the Linux-based cluster of the University of Bern (UBELIX) using 14 CPUs for the small CVEs and 64 CPUs for the large ones. The largest mesh contained 7.3 million elements and needed around 24 hours per load case.

2.3 Yield behavior of three samples under KUBCs- and PMUBCs-based embedded configuration for 17 load cases (Hypothesis I)

To check our first hypothesis, we evaluated the influence of the outer boundary conditions on the yield behavior of the embedded cubes. We thus computed the yield stresses and strains for three small CVEs embedded in large CVEs subjected to 17 load cases (Table 2) under KUBCs and PMUBCs (i.e., KUBCs- and PMUBCs-based embedded configurations) (Fig. 1b). The embedded cubes were chosen to feature low (6.5%), middle (14.1%), and high (32.2%) BV/TV (Table 1). We compared the impact of the two embedded configurations on each CVE by calculating the relative differences in yield stresses ($\sigma^{\mathrm{lc}}_{\mathrm{kubcs}}, \sigma^{\mathrm{lc}}_{\mathrm{pmubcs}}$) obtained for each load case (lc) taken individually ($\mathrm{diff}_{\mathrm{lc}}$) and all together ($\mathrm{diff}_{\mathrm{all}}$):

$$\mathrm{diff}_{\mathrm{lc}} = \frac{\sigma^{\mathrm{lc}}_{\mathrm{kubcs}} - \sigma^{\mathrm{lc}}_{\mathrm{pmubcs}}}{\sigma^{\mathrm{lc}}_{\mathrm{kubcs}}} \tag{2.3.1}$$

$$\mathrm{diff}_{\mathrm{all}} = \sum_{\mathrm{lc}=1}^{17} |\mathrm{diff}_{\mathrm{lc}}| \tag{2.3.2}$$

For visualization purposes, these 17 yield stresses were also used for fitting a BV/TV- and fabric-based generalized anisotropic quadric yield surface in normalized stress space (Schwiedrzik et al. 2013). (Levrero-Florencio et al. 2016) showed that fitting a yield surface to those 17 load cases or to 160 load cases provides equivalent results.

2.4 Yield behavior of 13 samples under KUBCs, PMUBCs and PMUBCs-based embedded configuration for six load cases (Hypothesis II)

To verify the second hypothesis, we assessed the effect of the BCs on the apparent yield properties of trabecular bone cubes. In our previous section, 17 load cases were conducted on three CVEs. Due to the high computational resources needed to test large CVEs, we applied only six load cases—tensile along $\mathbf{e}_3$ (tens3), compression along $\mathbf{e}_3$ (comp3), shear in the $\mathbf{e}_1$–$\mathbf{e}_2$ plane (shr12), shear in the $\mathbf{e}_2$–$\mathbf{e}_3$ plane (shr23), triaxial tension (ttens), and triaxial compression (tcomp) (Table 2)—to the 13 small CVEs under KUBCs, PMUBCs and embedded configuration (Fig. 1c). PMUBCs were chosen for the embedded configuration. This choice was not trivial as it was still not clear whether KUBCs and PMUBCs applied on the large CVEs would lead to the same yield stresses for the small embedded CVEs (Hypothesis I). However, prior results showed that thinner outer layers were required for PMUBCs-based elastic properties to converge toward the estimated effective properties (Daszkiewicz et al. 2017).

The yield stresses and strains were then computed for each BC and each CVE. KUBCs- and PMUBCs-based yield stresses were compared to embedded yield stresses in log space and linear regression, coefficient of determination (R^2) and root mean square error (RMSE) were computed. A one-way analysis of covariance (ANCOVA) was used to establish whether the linear relationships obtained between yield stresses and BV/TV were significantly affected by the BCs.

Mean yield strain over all 13 samples and the corresponding standard deviation (SD) and coefficient of variation (CV) were calculated for the six load cases under KUBCs, PMUBCs and embedded configuration. A one-way analysis of variance (ANOVA) was conducted to detect significant differences between yield stresses of the three BCs. All statistical analyses were performed with the statistics toolbox of MATLAB (R2014a).

2.5 Computation of the mean damage at yield point for six load cases (Hypothesis III)

A scalar damage variable (D) based on the cumulated plastic strain κ of the constitutive model (Schwiedrzik and Zysset 2013) was calculated to generate maps of tissue damage bounded by 0 (intact) and 1 (completely failed):

$$D(\kappa) = 1 - e^{-\kappa_p \kappa} \tag{2.5.1}$$

with κ_p being a constant material parameter (κ_p = 10.5). A FEAP routine was adapted to compute the damage value of each element (D_{ele}) according to Eq. 2.5.1 and based on a κ value averaged over the eight integration points (ipoint) of the finite element:

$$\kappa = \frac{1}{8} \sum_{\text{ipoint}=1}^{8} \kappa_{\text{ipoint}} \tag{2.5.2}$$

The mean damage (D_{mean}) under KUBCs, PMUBCs, and embedded configuration was computed in percent for the whole FE model at the yield point:

$$D_{\text{mean}} = \frac{1}{\text{number of elements}} \sum_{\text{ele}=1}^{\text{number of elements}} D_{\text{ele}} \times 100 \tag{2.5.3}$$

Finally, a one-way ANCOVA was used to establish whether the linear relationships obtained between D_{mean} and BV/TV were significantly affected by the BCs.

3 Results

3.1 Influence of outer boundary conditions on the yield behavior of the embedded cubes (Hypothesis I)

The largest differences between the yield stresses of the two embedded configurations were observed for sample 1 (the most porous of the three) with diff_{lc} up to 65% (Fig. 3). The differences measured for the two other samples were generally below 20%. Except for the triaxial compression on sample 3, the off-axis shear (shr23) seemed to be inducing the highest differences between KUBCs- and PMUBCs-based yield stresses. Overall, the impact of the outer BCs was relatively low when the sample was not too porous, but there was no clear relationship with BV/TV ($\text{diff}_{\text{all}} < 9\%$ for samples 2 and 3, but $\text{diff}_{\text{all}} = 28.21\%$ for sample 1).

3.2 Differences induced by KUBCs, PMUBCs, and PMUBCs-based embedded configuration on the yield stresses and yield strains (Hypothesis II)

In log space, KUBCs and PMUBCs yield stresses computed for uniaxial, multi-axial, and shear load cases were all linearly related to those resulting from PMUBCs-based embedded configuration ($R^2 > 0.96$ for KUBCs, $R^2 > 0.98$ for PMUBCs) (Fig. 4). Yet, among the three conditions, PMUBCs led to the lowest ($-10.0\% \pm 11.2\%$ compared to embedded), while KUBCs led to the highest yield stresses ($+43.1 \pm 27.9\%$ compared to embedded). The one-way ANCOVA confirmed significant differences between the yield stresses obtained from PMUBCs-based embedded configuration and direct KUBCs for comp3, shr12, shr23, ttens, and tcomp ($p < 0.05$), but no significant differences could be observed between PMUBCs-based embedded configuration and direct PMUBCs for any of the load cases. The KUBCs and PMUBCs yield stresses of all six load cases showed significant differences ($p < 0.05$).

In terms of yield strains (Table 3), the highest variations across the sample set were found for PMUBCs with a coefficient of variation (CV) up to 33% under ttens, while KUBCs yield strains had the lowest variation (CV < 9.5%). Under PMUBCs-based embedded configuration, CV ranged between 5.2 and 20.1%. Still, significant differences ($p < 0.05$) could only be observed for tcomp between KUBCs and PMUBCs-based embedded configuration and between KUBCs and PMUBCs.

3.3 Differences induced by KUBCs, PMUBCs, and PMUBCs-based embedded configuration on the computed mean damage (Hypothesis III)

Independently of the applied BCs, the mean damage was significantly increasing with BV/TV for each load case (Fig. 5).

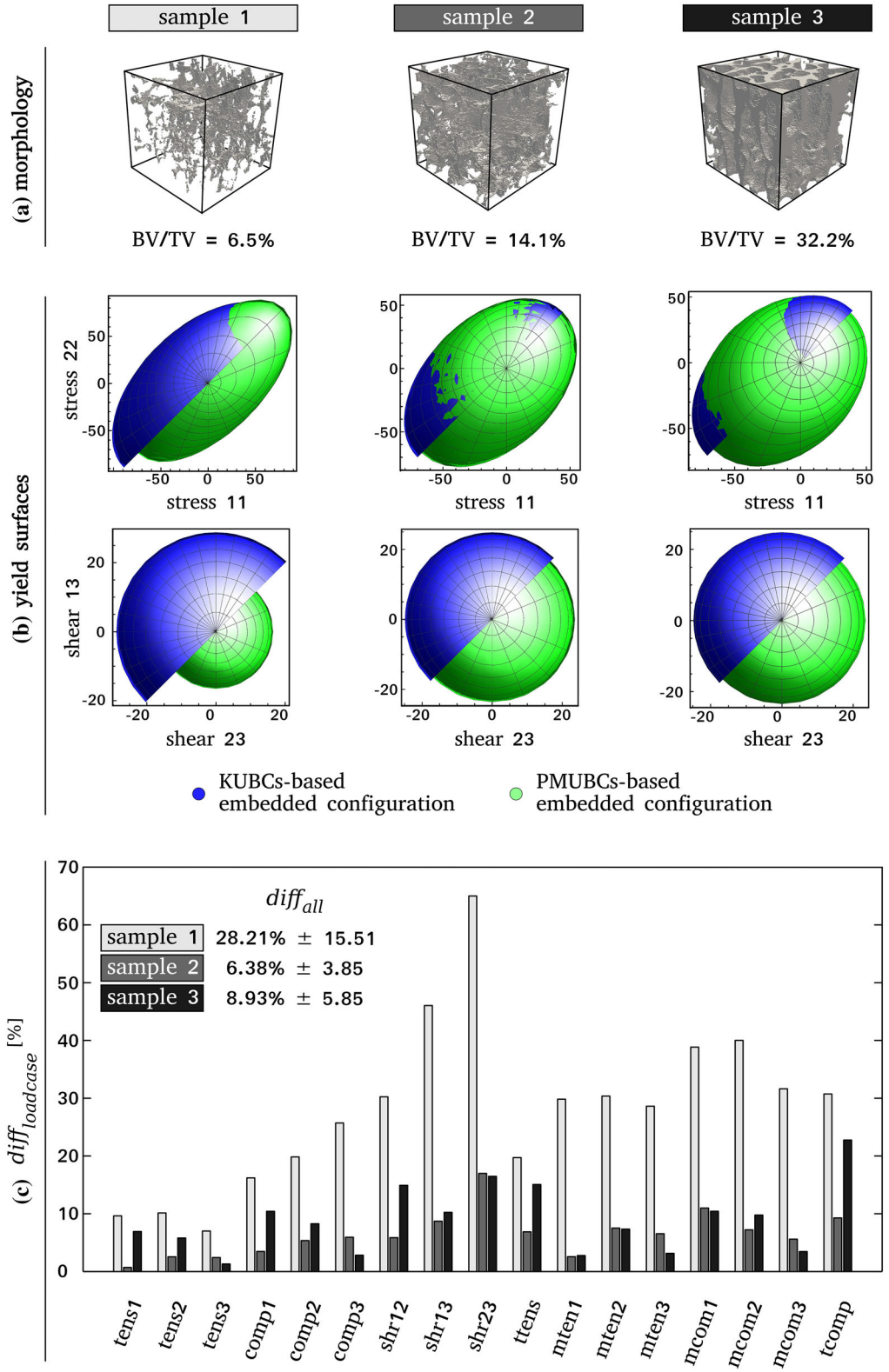

Fig. 3 **a** Three different CVEs were tested under KUBCs- and PMUBCs-based embedded configuration for 17 load cases. **b** Yield surfaces were fitted to the resulting yield stresses to visualize their differences. **c** The relative differences between KUBCs- and PMUBCs-based embedded yield stresses ($diff_{lc}$) were higher under shear. Yet, impact of the outer BCs ($diff_{all}$) was relatively low for samples 2 and 3

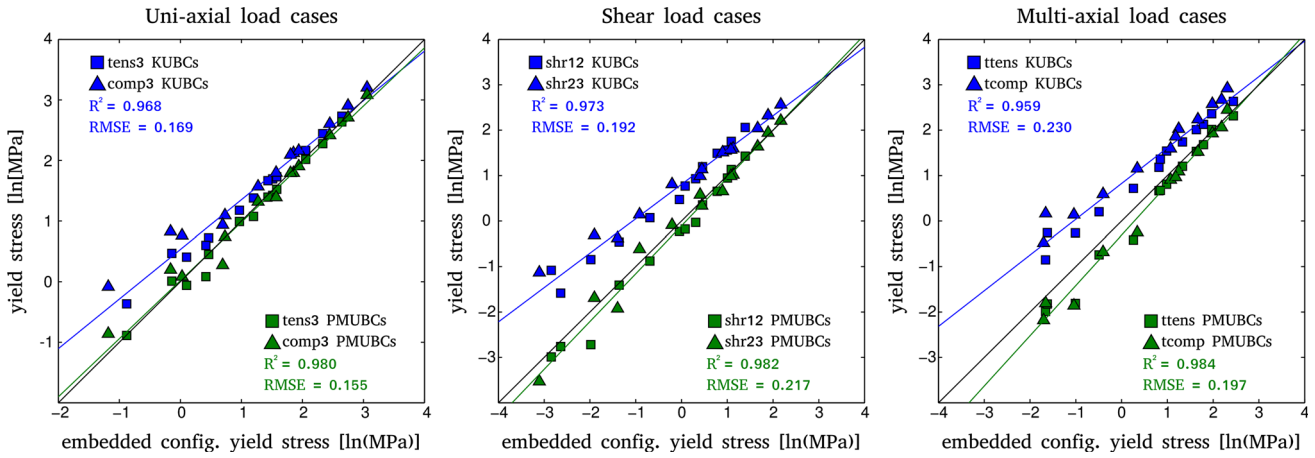

Fig. 4 In log space, the yield stresses obtained from KUBCs (*blue*) and PMUBCs (*green*) directly applied to the 13 CVEs linearly correlated with those obtained under embedded configuration

Table 3 Mean yield strain, standard deviation (SD), and coefficient of variation (CV) over all 13 samples under KUBCs, PMUBCs-based embedded configuration and PMUBCs for six load cases

Load case	KUBCs		Embedded		PMUBCs	
	Yield strain ± SD (%)	CV (%)	Yield strain ± SD (%)	CV (%)	Yield strain ± SD (%)	CV (%)
tens3	0.772 ± 0.045	5.8	0.779 ± 0.041	5.2	0.777 ± 0.085	10.9
comp3	1.042 ± 0.076	7.3	0.951 ± 0.125	13.1	0.982 ± 0.093	9.5
shr12	1.073 ± 0.059	5.5	1.236 ± 0.154	12.4	1.147 ± 0.266	23.2
shr23	1.015 ± 0.062	6.1	1.182 ± 0.177	15.0	1.026 ± 0.338	33.0
ttens	0.847 ± 0.080	9.5	0.899 ± 0.181	20.1	0.952 ± 0.297	31.2
tcomp	1.230* ± 0.061	5.0	1.050 ± 0.115	11.0	1.099 ± 0.149	13.5

Only yield strains obtained under KUBCs and tcomp were significantly different from those obtained under the other BCs (*)

Overall, KUBCs led to significantly higher mean damage compared to PMUBCs (+51.0 ± 16.9%) and embedded configuration (+48.4 ± 15.0%) ($p < 0.05$). However, significant differences could only be observed for shr23 between PMUBCs and PMUBCs-based embedded mean damage.

4 Discussion

Homogenizing non-periodic materials leads to apparent mechanical properties that are depending on the applied boundary conditions for VEs of limited size. Such dependency is not specific to bone and applies to porous and composite materials. Inspired by techniques used to alleviate the issue in continuum mechanics (Böhm 2016), Daszkiewicz et al. (2017) proposed an embedded cell approach to estimate the effective elastic properties of trabecular bone volumes. The current study is an extension of Daszkiewicz et al. (2017)'s pioneer work and focused on evaluating the effective yield properties of the same bone samples.

To our knowledge, this is the first time that the concept of embedded configuration is applied to nonlinear μFE analyses to estimate effective yield properties of trabecular VEs. Obviously, embedded configuration and multiple destructive loadings on a sample cannot be performed experimentally. Additionally, several routines of the original FE solver were adapted to provide the extent of damage within the samples in addition to yield stresses and strains. The samples, also used in Daszkiewicz et al. (2017), featured a broad range of density and morphology (BV/TV ranges from 6.5 to 32.2%). Extra verifications such as the validity of Hill's condition matching the energy density at the micro- and macro-level ("Appendices: Fig. 6") and the impact of the voxel size on the yield stresses and strains were evaluated ("Appendices: Fig. 7").

Hypothesis I was that the yield properties obtained from embedded samples are independent of the outer BCs if the surrounding layer is thicker than 2 mm (Fig. 1b). Hypothesis I is accepted, under the condition that the sample is not too porous (BVTV > 6.5%). Only three samples out of 13 were tested under both KUBCs- and PMUBCs-based embedded configuration with 17 load cases because of the large computational resources needed for running such simulations. The resulting yield stresses were compared between the two con-

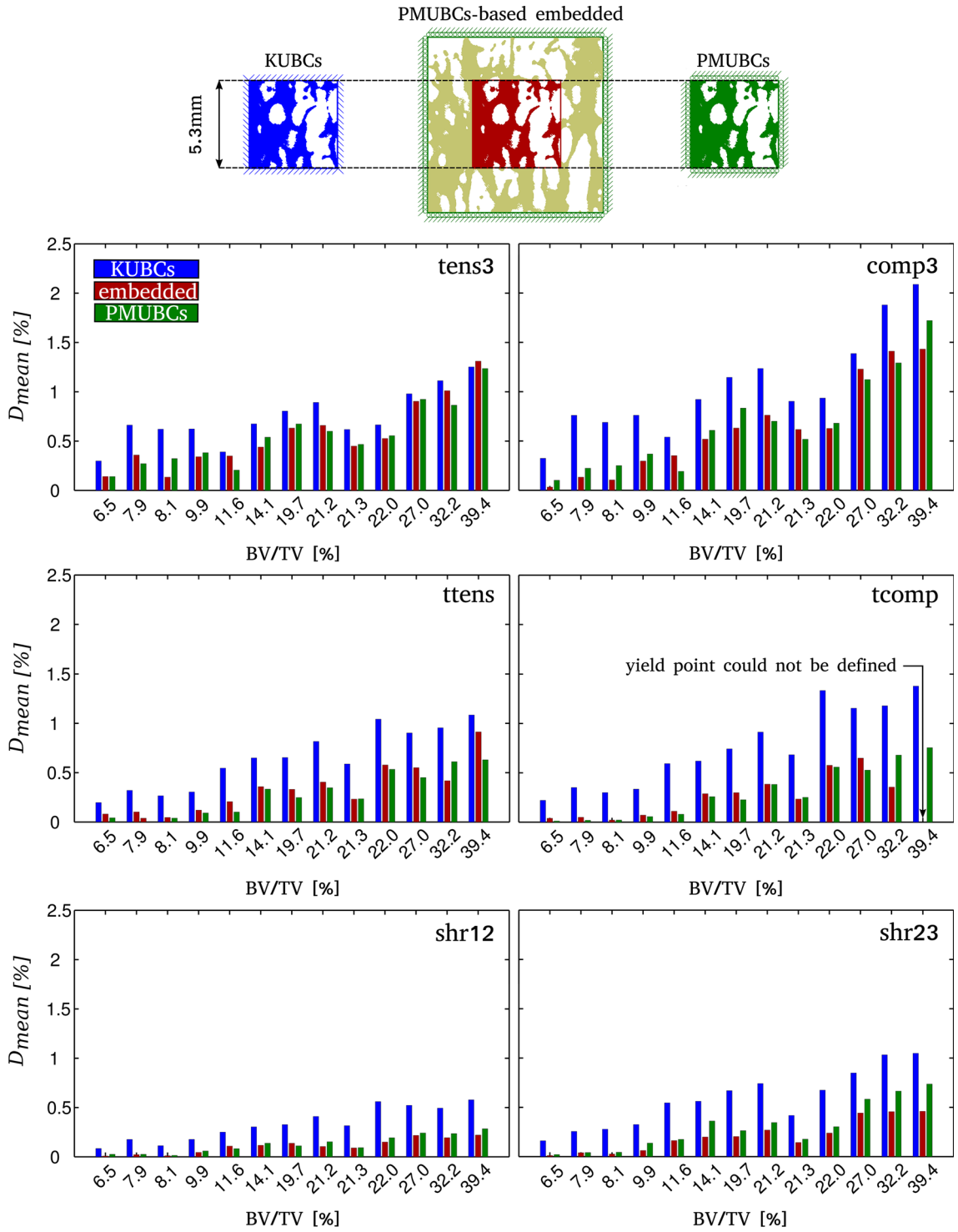

Fig. 5 Comparison between the mean damage (D_{mean}) obtained under KUBCs (*blue*), embedded configuration (*red*) and PMUBCs (*green*) for the 13 samples under six load cases

figurations and could be successfully fitted to individual yield surfaces. Analogue to elasticity (Daszkiewicz et al. 2017, the effect of the BCs on the yield behavior of the embedded cube almost vanishes for a layer thickness of 2.65 mm, but only if BV/TV is large enough. Indeed, our most porous sample (sample 1, BV/TV = 6.5%) remained affected by the outer BCs, especially under shear and multi-axial compressions. Unlike PMUBCs, KUBCs do not allow the trabeculae to deform freely, thus artificially reinforcing their contribution to the overall mechanical behavior (Pahr and Zysset

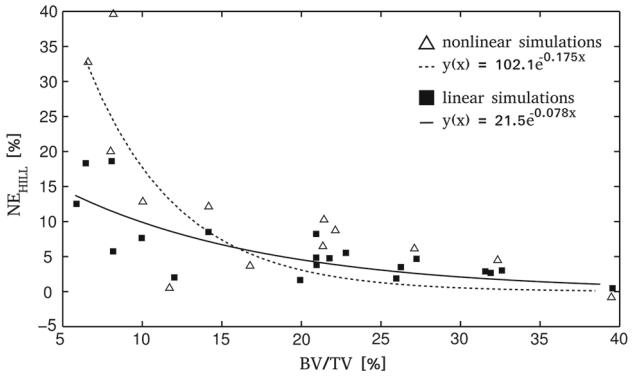

Fig. 6 The normalized difference between micro- and macro-level strain energies (NE_{HILL}) was computed to check the validity of Hill's condition for the nonlinear analysis of the PMUBCs-based embedded configuration (*triangles*). NE_{HILL} obtained previously from the linear analyses (Daszkiewicz et al. 2017) were also plotted for comparisons (squares). $NE_{HILL} = \frac{1}{LC}\sum_{l=1}^{LC}\left(\frac{1}{nstep}\sum_{step=1}^{nstep}\frac{|\sigma:\varepsilon^{step}-\sigma^{step}:\varepsilon^{step}|}{\sigma^{step}:\varepsilon^{step}}\right)$, where LC is the number of load cases (6), nstep is the number of steps required for the load case (l) to reach the yield point (σ, ε)

2008). This explains why just few rod-like trabeculae surrounding sample 1 better transmit the deformations from the outer layer when KUBCs are applied. Nevertheless, exactly because PMUBCs are more compliant, we can reasonably assume that PMBCs-based embedded configuration lead to the effective yield properties as demonstrated for elasticity (Jiang et al. 2001; Blöß and Welsch 2015; Daszkiewicz et al. 2017).

Hypothesis II was that PMUBCs are able to mimic the yield stresses obtained from the embedded configuration better than KUBCs (Fig. 1c). Hypothesis II is accepted for both yield stresses and strains. All 13 samples were tested under KUBCs, PMUBCs, and PMUBCs-based embedded configuration for two uniaxial, two shear and two multi-axial load cases. Consistent with earlier results pertaining to elasticity (Daszkiewicz et al. 2017), the findings demonstrate that compliant PMUBCs indeed provide a better estimation of the embedded yield stresses than the strict KUBCs. In most cases, PMUBCs even slightly underestimated the embedded yield stresses, especially for low BV/TV, but the differences were not significant. As expected, KUBCs overestimated significantly the embedded values, except for tens3. This is not surprising considering that tens3 is a uniaxial tension along the main trabecular axis (more & larger trabeculae in this direction) and that KUBCs' overestimation decreases with higher BV/TV (Pahr and Zysset 2008). Contrary to yield stress, no significant differences could be found between the yield strains obtained with the three BCs. This was already demonstrated by Panyasantisuk et al. (2016) between KUBCs and PMUBCs yield strains, but never for CVE loaded "in situ". The mean yield strains under KUBCs and PMUBCs are slightly lower in the shear and tensile cases compared to the embedded configuration. Bone tissue yields more easily under shear and tension, but the CVE is "protected" by the surrounding layer of bone compared to a direct loading. Nevertheless, our finding confirms that yield strains are fairly independent of the BCs and can be used as a yield criteria.

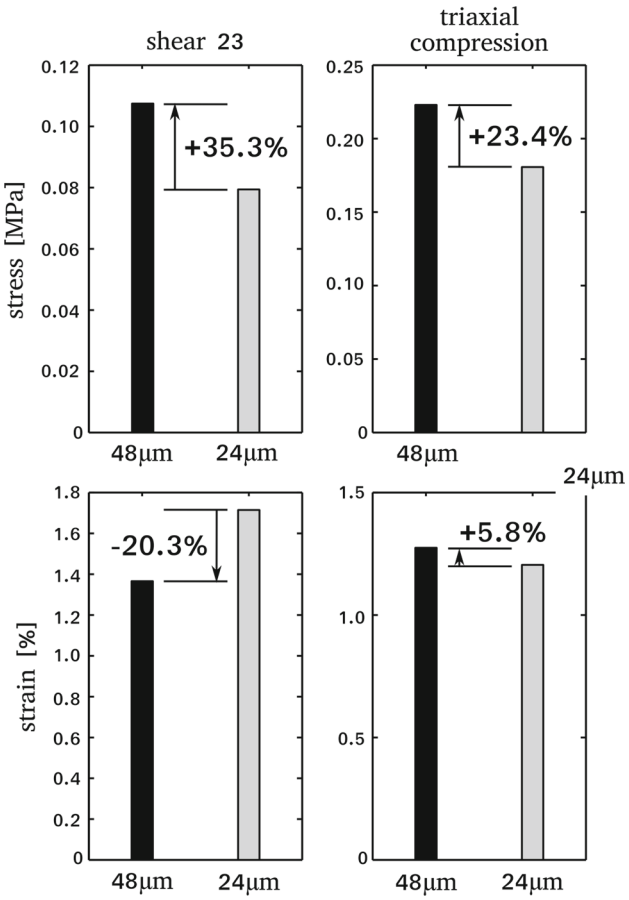

Fig. 7 Differences in yield stress and yield strain due to the voxel size for the most sensitive sample (BV/TV=6.3%) under embedded configuration.

Hypothesis III was that PMUBCs induce similar damage distribution as the embedded configuration, unlike KUBCs (Fig. 1d). Hypothesis III is also confirmed. The computed damage followed similar trends as the yield stresses. The mean damage level under PMUBCs was closer to the embedded configuration, than the ones under KUBCs. Overall, samples undergo more damage under KUBCs than under PMUBCs and embedded configuration, even though the used damage model is strain-driven and the differences in the yield strains are rather small. However, KUBCs do not let trabeculae (even the thin and fragile ones) deform freely. This led to higher damage very close to the boundary compared to the rest of the cube, which indicates that regions close to the surface undergoes high strain under KUBCs.

Several limitations of this study should be underlined. The morphological parameters of the large and embedded CVEs are not rigorously identical (Table 1), which points to the intrinsic heterogeneous nature of human trabecular bone and

the difficulty to determine an RVE. Hill's condition is not exactly fulfilled ("Appendices: Fig. 6") and numerical errors may influence the results (Blöss and Welsch 2015). Still, the errors of the nonlinear analyses are in the same range as they are for linear analyses, even for samples with BV/TV lower than 10% (Daszkiewicz et al. 2017). Our conclusions are likely not affected given the comparative nature of the study. The voxel size also has a large impact on the yield stress and yield strain computed with nonlinear μFE ("Appendices: Fig. 7"). Yet, Bevill and Keaveny (2009) showed that yield stresses estimated with 80 μm voxel size correlated highly with estimations made using 20 μm voxel size. Only three samples were tested under both embedded configurations. CVE large enough for the embedded configuration could not be extracted from other relevant locations such as patella (Latypova et al. 2016) and distal radius (Hosseini et al. 2017). The yield point of one sample (BV/TV=39.4%) could not be reached for triaxial compression (tcomp) under embedded configuration. The outer layer of this sample was more porous than its core and yielded before the embedded CVE.

In this study, the embedding technique, as well as visualization and evaluation of the computed damage, was successfully adapted to nonlinear μFE simulations. Embedded yield properties were shown to be nearly independent of the type of boundary conditions, at least for samples that are not excessively porous. The embedded configuration can therefore, under certain conditions (porosity, thickness of the outer layer), approximate the effective yield properties of trabecular bone. As in the elastic case, PMUBCs provided yield properties close to those obtained with embedded configurations. This confirms early assumptions that PMUBCs could mimic the real deformations applying on a trabecular VE sufficiently far from the cortex. In further studies, PMUBCs can thus reasonably be used instead of the computationally demanding embedded situation for evaluating effective properties of trabecular bone. The accuracy of these effective yield properties will have to be checked against the homogenization of very high-resolution images ($\leq$12 μm) under embedded configuration, but this will require tremendous computing power.

Acknowledgements The authors thank Bert van Rietbergen (Eindhoven University of Technology, Netherlands) for providing the μCT data and Karol Daszkiewicz (Gdansk, University of Technology, Poland) for his support. This work was funded by the Gebert Rüf Foundation (GRS-079/14) and the Swiss National Science Foundation (Grant no. 143769).

Compliance with ethical standard

Conflict of interest The authors declare that they have no conflict of interest.

References

Bayraktar HH, Morgan EF, Niebur GL, Morris GE, Wong EK, Keaveny TM (2004) Comparison of the elastic and yield properties of human femoral trabecular and cortical bone tissue. J Biomech 37(1):27–35

Bevill G, Keaveny TM (2009) Trabecular bone strength predictions using finite element analysis of micro-scale images at limited spatial resolution. Bone 44(4):579–584

Blöß T, Welsch M (2015) RVE Procedure for Estimating theElastic Properties of Inhomogeneous Microstructures Such as BoneTissue. Biomedical Technology 74:1–17. Springer

Böhm HJ (2016) A short introduction to basic aspects of continuum micromechanics, CDL–FMD Report 3–1998, TU Wien, Vienna.http://www.ilsb.tuwien.ac.at/links/downloads/ilsbrep206.pdf

Cowin SC (1985) The relationship between the elasticity tensor and the fabric tensor. Mech Mater 4:137–147

Daszkiewicz K, Maquer G, Zysset PK (2017) The effective elastic properties of human trabecular bone may be approximated using micro-finite element analyses of embedded volume elements. Biomech Model Mechanobiol 16(3):731–742

Harrigan TP, Mann RW (1984) Characterization of microstructural anisotropy in orthotropic materials using a second rank tensor. J Mater Sci 19(3):761–767

Harrigan TP, Jasty M, Mann RW, Harris WH (1988) Limitations of the continuum assumption in cancellous bone. J Biomech 21(4):269–275

Hazanov S, Huet C (1994) Order relationships for boundary conditions effect in heterogeneous bodies smaller than the representative volume. J Mech Phys Solids 42(12):1995–2011

Hill R (1963) Elastic properties of reinforced solids: some theoretical principles. J Mech Phys Solids 11:127–140

Hollister SJ, Fyhrie DP, Jepsen KJ, Goldstein SA (1991) Application of homogenization theory to the study of trabecular bone mechanics. J Biomech 24(9):825–839

Hosseini HS, Maquer G, Zysset PK (2017) μ CT-based trabecular anisotropy can be reproducibly computed from HR-pQCT scans using the triangulated bone surface. Bone 97:114–120

Jiang M, Alzebdeh K, Jasiuk I, Ostoja-Starzewski M (2001) Scale and boundary conditions effects in elastic properties of random composites. Acta Mech 148:63–78

Latypova A, Maquer G, Elankumaran K, Pahr D, Zysset P, Pioletti DP, Terrier A (2016) Identification of elastic properties of human patellae using micro-finite element analysis. J Biomech 49(13):3111–3115

Levrero-Florencio F, Margetts L, Sales E, Xie S, Manda K, Pankaj P (2016) Evaluating the macroscopic yield behaviour of trabecular bone using a nonlinear homogenisation approach. J Mech Behavior Biomed Mater 61:384–396

Lochmüller EM, Pöschl K, Würstlin L, Matsuura M, Müller R, Link TM, Eckstein F (2008) Does thoracic or lumbar spine bone architecture predict vertebral failure strength more accurately than density? Osteoporos Int 19(4):537–545

Maquer G, Musy SN, Wandel J, Gross T, Zysset PK (2015) Bone volume fraction and fabric anisotropy are better determinants of trabecular bone stiffness than other morphological variables. J Bone Mineral Res 30(6):1000–1008

Marangalou JH, Ito K, Cataldi M, Taddei F, van Rietbergen B (2013) A novel approach to estimate trabecular bone anisotropy using a database approach. J Biomech 46(14):2356–2362

Musy SN, Maquer G, Panyasantisuk J, Wandel J, Zysset PK (2017) Not only stiffness, but also yield strength of the trabecular structure determined by non-linear μFE is best predicted by bone volume

fraction and fabric tensor. J Mech Behavior Biomed Mater 65:808–813

Pahr DH, Zysset P (2008) Influence of boundary conditions on computed apparent elastic properties of cancellous bone. Biomech Model Mechanobiol 7(6):463–476

Panyasantisuk J, Pahr DH, Zysset PK (2016) Effect of boundary conditions on yield properties of human femoral trabecular bone. Biomech Model Mechanobiol 15(5):1043–1053

Qasim M, Farinella G, Zhang J, Li X, Yang L, Eastell R, Viceconti M (2016) Patient-specific finite element estimated femur strength as a predictor of the risk of hip fracture: the effect of methodological determinants. Osteoporos Int 27(9):2815–2822

Ray NF, Chan JK, Thamer M, Melton LJ (1997) Medical expenditures for the treatment of osteoporotic fractures in the United States in 1995: report from the National Osteoporosis Foundation. J Bone Mineral Res 12(1):24–35

Schwiedrzik JJ, Zysset PK (2013) An anisotropic elastic–viscoplastic damage model for bone tissue. Biomech Model Mechanobiol 12(2):201–213

Schwiedrzik JJ, Wolfram U, Zysset PK (2013) A generalized anisotropic quadric yield criterion and its application to bone tissue at multiple length scales. Biomech Model Mechanobiol 12(6):1155–1168

Schwiedrzik JJ, Gross T, Bina M, Pretterklieber M, Zysset P, Pahr D (2016) Experimental validation of a nonlinear FE model based on cohesive-frictional plasticity for trabecular bone. Int J Numer Methods Biomed Eng. doi:10.1002/cnm.2739

Taylor RL, Govindjee S (2013) FEAP a finite element analysis program. Parallel User Manual Version 8.4. University of California at Berkeley, Berkeley, California, USA. http://www.ce.berkeley.edu/projects/feap/parmanual.pdf

van Rietbergen B, Weinans H, Huiskes R, Odgaard A (1995) A new method to determine trabecular bone elastic properties and loading using micromechanical finite-element models. J Biomech 28(1):69–81

Zysset PK (2003) A review of morphology-elasticity relationships in human trabecular bone: theories and experiments. J Biomech 36(10):1469–1485

Zysset PK, Goulet RW, Hollister SJ (1998) A global relationship between trabecular bone morphology and homogenized elastic properties. J Biomech Eng 120(5):640–646

Zysset P, Qin L, Lang T, Khosla S, Leslie WD, Shepherd JA, Engelke K (2015) Clinical use of quantitative computed tomography-based finite element analysis of the hip and spine in the management of osteoporosis in adults: the 2015 ISCD official positions-part II. J Clin Densitom 18(3):359–392